

# Improved Sliding Mode Observer for Position Sensorless Open-Winding Permanent Magnet Brushless Motor Drives

Qing Lu<sup>1, 2</sup>, Li Quan<sup>1, \*</sup>, Xiaoyong Zhu<sup>1</sup>, Yuefei Zuo<sup>1</sup>, and Wenye Wu<sup>1</sup>

**Abstract**—To enhance the accuracy of estimated rotor position for sensorless controlled permanent magnet synchronous motor, the strategy based on sliding mode observer (SMO) with dual second order generalized integrator (DSOGI) is proposed. The SMO is utilized to estimate the back electromotive force (EMF). Considering the estimated back-EMF harmonics resulting from both flux spatial harmonics and inverter nonlinearities, the DSOGI is applied to eliminate multiple orders harmonics and extract the fundamental wave of the estimated back-EMF for calculating the rotor position. Therefore, the DSOGI can effectively reduce the influence of the estimated back-EMF harmonics and improve the accuracy of rotor position estimation. In addition, the software quadrature phase-locked loop with back-EMF normalization is utilized to calculate the rotor position in order to eliminate the influence of the changed back-EMF magnitude at different speed. Finally, to illustrate the effectiveness of the proposed strategy, the experimental platform of an open-winding permanent magnet brushless motor is built. The comparison results verified that the drive system performance of both steady state and dynamic state is improved.

## 1. INTRODUCTION

Permanent magnet brushless motor has been widely used in many industrial applications due to its advantageous features, such as small size, low cost, high power density, and high efficiency [1–4]. Open-winding permanent magnet brushless motor not only has the advantages of traditional permanent magnet brushless motor, but also improves the efficiency and stability of the drive system, and reduces the capacity of single inverter. Open-winding technology has attracted more and more attention in recent years [5, 6].

Like the closed-loop vector control system of the traditional motor, rotor position is also necessary for the high performance control system of open-winding permanent magnet brushless motor. However, utilization of additional mechanical position sensors not only decreases the systematic reliability but also increases the system complexity and cost. Consequently, the sensorless control technique, which can obtain the position information by easily measured voltage and current signals, has become one of the research focuses in the field of motor control [7–9].

According to speed region, the reported sensorless control methods can be classified into two categories: high frequency signal injection methods and the model-based methods [10–13]. The former, which obtains rotor position information by salient pole of motor, is suitable for low and zero speed operating motor. The latter that estimates rotor position through fundamental model is adopted for the medium and high speed operating motor. High frequency signal injection method mainly includes: high frequency pulsating voltage injection method, high frequency rotating voltage injection method, high frequency pulsating current injection method, high frequency square wave voltage injection method

---

*Received 5 November 2018, Accepted 14 December 2018, Scheduled 3 January 2019*

\* Corresponding author: Li Quan (quanliemail@126.com).

<sup>1</sup> School of Electrical and Information Engineering, Jiangsu University, Zhenjiang 212013, China. <sup>2</sup> Faculty of Automation, Huaiyin Institute of Technology, Huai'an 221200, China.

and so on [10,11]. The model-based methods mainly include the disturbance observer, the sliding mode observer (SMO), extended state observer, the Kalman filtering method, model reference adaptive observer, etc. [12,13]. However, back-EMF estimation error usually happens in the SMO method, and the accuracy of estimated rotor position is decreased. The estimated error includes a dc drift and a harmonic fluctuation component. The dc drift is resulted from parameter uncertainties and can be reduced by parameter identification. The fluctuation components exist in the estimated back-EMF due to the flux spatial harmonics and the inverter nonlinearities. In order to reduce the influence of the harmonic fluctuations, various compensation methods for the harmonics of the back-EMF estimation have been proposed.

In [14], a revised repetitive controller is proposed to suppress the dead-time distortion, and the estimation error can be reduced. However, it only eliminates the harmonics resulting from the inverter nonlinearities. In [15], Lin et al. analyzed the back-EMF harmonics of a switched-flux motor and utilized an adaptive notch filter to eliminate the flux estimation harmonics. In [16], Zhang et al. used multiple adaptive vector filters to eliminate the specific harmonics in position estimation error due to the inverter nonlinearity and flux spatial harmonics. The proposed methods in [15] and [16] can be used to eliminate the specific harmonics. Nevertheless, the above methods need to add multiple filters according to the harmonic orders. It is a great challenge to propose a strategy can eliminate random harmonic error if the estimated back-EMF contains multiple orders harmonics. The dual second order generalized integrator (DSOGI) has been used in the power system to eliminate the current harmonics [17,18]. Also, the DSOGI can be used in the rotor position observer to reduce the back-EMF harmonics.

The main purpose of this paper is to propose a revised rotor position observer with DSOGI to achieve high accuracy rotor position estimation for the open-winding permanent magnet brushless motor, whose estimated back-EMF exhibits non-sinusoidal characteristics. The DSOGI is used to eliminate the harmonics and extract the fundamental wave of estimated back-EMF for the rotor position calculation. First of all, the topology of the open-winding permanent magnet brushless motor drive system is briefly depicted in Section 2. Then, the traditional rotor position estimation method based on SMO for interior permanent magnet synchronous motor (IPMSM), the main strategy of the proposed DSOGI and the quadrature phase-locked loop (PLL) with back-EMF normalization are presented in Section 3. Finally, an experimental platform of the open-winding permanent magnet brushless motor is built in Section 4. The effectiveness and feasibility of proposed strategy are validated by the experimental results.

## 2. TOPOLOGY OF OPEN-WINDING MOTOR DRIVE SYSTEM

Open-winding topology includes two modes: the single DC power supply mode and dual DC power supply mode. The single DC power supply mode is adopted in this paper due to the simple structure, which is shown as Figure 1. The mathematical model of the motor in abc reference frame can be expressed as follows:

$$\begin{bmatrix} u_a \\ u_b \\ u_c \end{bmatrix} = \begin{bmatrix} e_a \\ e_b \\ e_c \end{bmatrix} + R \begin{bmatrix} i_a \\ i_b \\ i_c \end{bmatrix} + \frac{d}{dt} \left\{ \begin{bmatrix} L_{aa} & M_{ab} & M_{ac} \\ M_{ba} & L_{bb} & M_{bc} \\ M_{ca} & M_{cb} & L_{cc} \end{bmatrix} \begin{bmatrix} i_a \\ i_b \\ i_c \end{bmatrix} \right\} \quad (1)$$

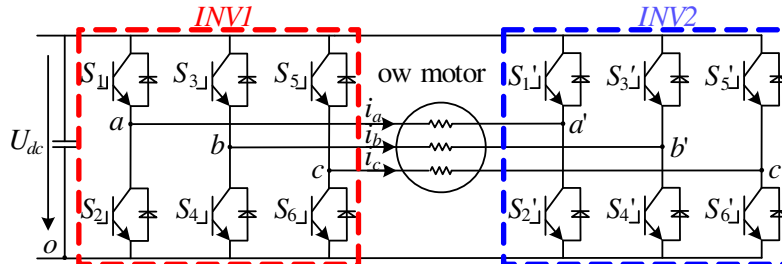


**Figure 1.** Open-winding motor drive system with single DC power supply.

$$\begin{bmatrix} e_a \\ e_b \\ e_c \end{bmatrix} = \frac{d}{dt} \begin{bmatrix} \psi_{fa} \\ \psi_{fb} \\ \psi_{fc} \end{bmatrix} \tag{2}$$

where  $u_a, u_b, u_c$  are the phase voltages;  $i_a, i_b, i_c$  are the phase currents;  $R$  is the stator resistance;  $L$  and  $M$  are self-inductance and mutual inductance, respectively;  $e_a, e_b, e_c$  are the back-EMFs;  $\psi_{fa}, \psi_{fb}, \psi_{fc}$  are the magnetic field linkage.

The two inverters are supplied by single DC power. The relationship between motor phase voltage and inverter output voltage can be expressed as follows:

$$\begin{bmatrix} u_a \\ u_b \\ u_c \end{bmatrix} = U_{dc} \begin{bmatrix} S_{a1} \\ S_{b1} \\ S_{c1} \end{bmatrix} - U_{dc} \begin{bmatrix} S_{a2} \\ S_{b2} \\ S_{c2} \end{bmatrix} \tag{3}$$

where  $S_{mx}$  is the switch function ( $x = 1, 2, m = a, b, c$ ), if the switch of upper bridge arm is turned on,  $S_{mx} = 1$ ; otherwise, if the switch of lower bridge arm is turned on,  $S_{mx} = 0$ ;  $U_{dc}$  is the DC power. Therefore, the inverter output voltage can be obtained by the switch stated. The mathematical model of the motor in  $d$ - $q$  frame can be expressed as follows:

$$\begin{bmatrix} u_d \\ u_q \end{bmatrix} = \begin{bmatrix} u_{d1} - u_{d2} \\ u_{q1} - u_{q2} \end{bmatrix} = \begin{bmatrix} R + L_d p & -\omega L_q \\ \omega L_d & R + L_q p \end{bmatrix} \begin{bmatrix} i_d \\ i_q \end{bmatrix} + \begin{bmatrix} 0 \\ \omega \psi_{f1} \end{bmatrix} \tag{4}$$

where  $u_d$  and  $u_q$  are the  $d$ - $q$ -axes voltages of open-winding motor;  $u_{d1}, u_{q1}$  and  $u_{d2}, u_{q2}$  are the  $d$ - $q$ -axes voltages of the two inverters, respectively;  $i_d$  and  $i_q$  are the  $d$ - $q$ -axes currents;  $L_d$  and  $L_q$  are the  $d$ - $q$ -axis inductances;  $\psi_{f1}$  is the rotor flux linkage;  $\omega$  is the rotor electrical speed;  $p$  is the differential operator.

### 3. SENSORLESS CONTROL STRATEGY BASED ON SMO

Figure 2 shows the sensorless controlled open-winding PMSM based on revised SMO, which can improve the accuracy of estimated rotor position. It can be seen that the back-EMF estimation can be calculated by the sliding mode observer. Then, the DSOGI is adopted to extract the fundamental component of the back-EMF. Finally, the rotor position information can be estimated by the PLL using the fundamental component of the back-EMF.

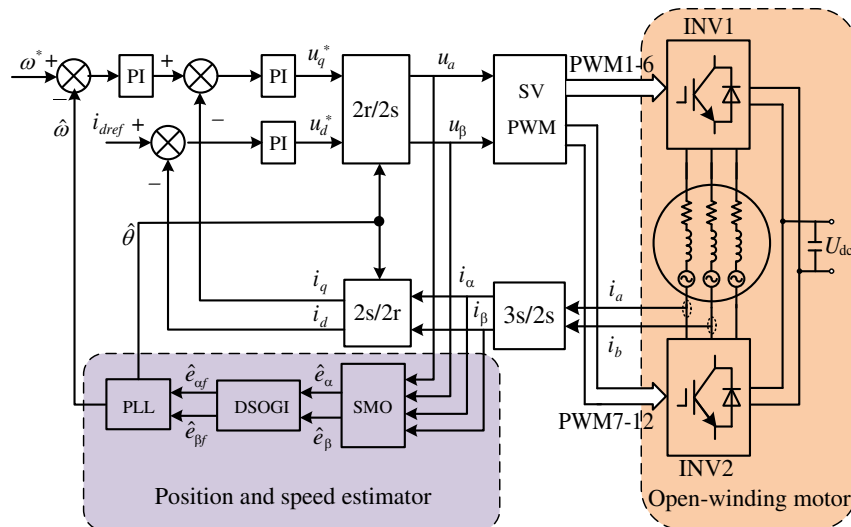


Figure 2. Sensorless control system of open-winding PMSM.

#### 3.1. IPMSM Rotor Position Estimation Scheme Based on SMO

In order to design the SMO for estimating the rotor position and speed, the mathematical model of the motor can be transformed to the equation in  $\alpha$ - $\beta$  stationary frame. Consequently, the mathematical

model of IPMSM in  $\alpha$ - $\beta$  stationary frame can be written as follows

$$\begin{bmatrix} u_\alpha \\ u_\beta \end{bmatrix} = \begin{bmatrix} R + pL_d & \omega(L_d - L_q) \\ -\omega(L_d - L_q) & R + pL_d \end{bmatrix} \begin{bmatrix} i_\alpha \\ i_\beta \end{bmatrix} + [\omega\psi_{f1} + (L_d - L_q)(\omega i_d - pi_q)] \begin{bmatrix} -\sin\theta \\ \cos\theta \end{bmatrix} \quad (5)$$

where  $u_\alpha$ ,  $u_\beta$  and  $i_\alpha$ ,  $i_\beta$  are the  $\alpha$ - $\beta$ -axis voltages and currents, and  $\theta$  is the rotor position. The extended back-EMF [19] equation of IPMSM is defined as

$$E_{ext} = \begin{bmatrix} e_\alpha \\ e_\beta \end{bmatrix} = [\omega\psi_{f1} + (L_d - L_q)(\omega i_d - pi_q)] \begin{bmatrix} -\sin\theta \\ \cos\theta \end{bmatrix} \quad (6)$$

where  $e_\alpha$  and  $e_\beta$  are the  $\alpha$ - $\beta$ -axis back-EMF components. From Equations (5) and (6), it is obvious that the extended back-EMF contains rotor position  $\theta$ . If the extended back-EMF is obtained, the rotor position can be estimated. So the extended back-EMF should be estimated firstly. In order to obtain the extended back-EMF, the mathematical model of IPMSM in  $\alpha$ - $\beta$  stationary frame can be rewritten as follows

$$\frac{d}{dt} \begin{bmatrix} i_\alpha \\ i_\beta \end{bmatrix} = A \begin{bmatrix} i_\alpha \\ i_\beta \end{bmatrix} + \frac{1}{L_d} \begin{bmatrix} u_\alpha \\ u_\beta \end{bmatrix} - \frac{1}{L_d} \begin{bmatrix} e_\alpha \\ e_\beta \end{bmatrix} \quad (7)$$

where

$$A = \frac{1}{L_d} \begin{bmatrix} -R & -\omega(L_d - L_q) \\ \omega(L_d - L_q) & -R \end{bmatrix}.$$

Both the voltage and current are easily measured in the motor control system. According to the sliding mode theory, the  $S = \hat{i} - i = 0$  can be selected as the sliding mode surface. The sign “ $\hat{\cdot}$ ” denotes estimation. The current can be estimated by the observer. Therefore, the mathematical model of the current observer can be written as

$$\frac{d}{dt} \begin{bmatrix} \hat{i}_\alpha \\ \hat{i}_\beta \end{bmatrix} = A \begin{bmatrix} \hat{i}_\alpha \\ \hat{i}_\beta \end{bmatrix} + \frac{1}{L_d} \begin{bmatrix} u_\alpha \\ u_\beta \end{bmatrix} - \frac{1}{L_d} k \begin{bmatrix} H_\alpha \\ H_\beta \end{bmatrix} \quad (8)$$

where  $k$  is the observer gain;  $H$ ,  $H_\alpha$ , and  $H_\beta$  are the equivalent control value and the  $\alpha$ - $\beta$ -axis components, respectively. According to the SMO theory, to ensure the existence and stability of sliding motion, the observer gain  $k$  should meet the requirement:  $k > \max(|e_\alpha|, |e_\beta|)$ .

In the conventional structure of SMO, the simple sign function is selected as switching function. However, the simple sign function will result in high frequency chattering. To eliminate the high frequency chattering, the sigmoid function, which is defined as Eq. (9), can replace the sign function.

$$\text{sigmoid} = \frac{2}{1 + e^{-ax}} - 1. \quad (9)$$

The back-EMF estimation is contained in the switching control function. In addition, the switching control function also contains high frequency components. Therefore, the LPF is selected to suppress the high frequency components, and the back-EMF estimation is obtained as follow.

$$\begin{bmatrix} e_\alpha \\ e_\beta \end{bmatrix} = \text{LPF} \begin{bmatrix} kH_\alpha \\ kH_\beta \end{bmatrix} \quad (10)$$

where LPF is the low-pass filter.

Conventionally, the rotor position estimation can be calculated directly from the estimated back-EMF using an arc-tangent function as

$$\hat{\theta} = -\arctan(\hat{e}_\alpha/\hat{e}_\beta) \quad (11)$$

The block of rotor position estimation method based on the traditional SMO is shown in Figure 3.

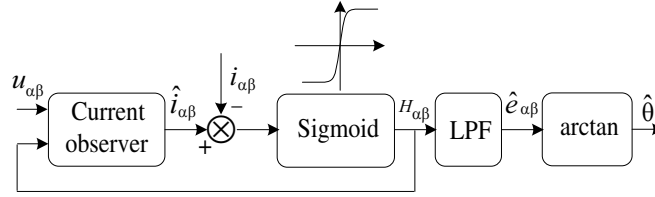


Figure 3. Block diagram of traditional SMO system.

### 3.2. PLL with Back-EMF Normalization

In the traditional observer, the arc-tangent function can be utilized to calculate the rotor position estimation. However, to eliminate the influence of harmonics and high frequency chattering, the rotor position is calculated by a quadrature PLL with back-EMF normalization, which is shown in Figure 4. Furthermore, the transfer function can be expressed as

$$G_{PLL} = \frac{\hat{\theta}_e}{\theta_e} = \frac{k_p s + k_i}{s^2 + k_p s + k_i} \quad (12)$$

where  $1/s$  is the integral function,  $k_p$  the proportion coefficient, and  $k_i$  the integral coefficient in the PLL. The output of back-EMF normalization function is used as the input of PLL. Then, the PLL can calculate the rotor position and speed.

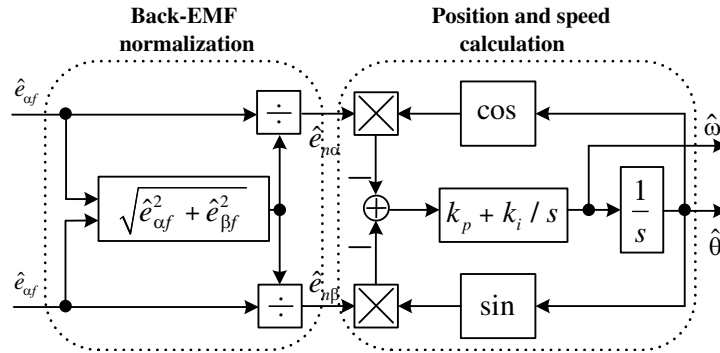


Figure 4. PLL with back-EMF normalization.

It can be seen from Eq. (12) that the PLL with back-EMF normalization is not influenced by the back-EMF amplitude. Therefore, the PLL can be applicable to different speeds. The rotor position can be calculated by the normalized back-EMF as

$$\hat{\theta} = (1/s)(k_i/s + k_p)(-\hat{e}_\alpha \cos \hat{\theta} - \hat{e}_\beta \sin \hat{\theta}) \left(1/\sqrt{\hat{e}_\alpha^2 + \hat{e}_\beta^2}\right) \quad (13)$$

### 3.3. SMO with DSOGI and PLL

Due to the influence of flux spatial harmonics and inverter nonlinearity, the estimated back-EMF exhibits non-sinusoidal characteristics. The harmonic components will result in fluctuation error in the estimated rotor position. Therefore, it is necessary to suppress the harmonics.

The revised position observer with detailed diagram of DSOGI is shown in Figure 5. It can be seen that the observer includes SMO unit, DSOGI unit and PLL unit. The SMO is used to estimate the original back-EMF. Then the DSOGI can eliminate the harmonics and extract the fundamental component of back-EMF for calculating rotor position. The PLL with normalization can eliminate the influence of the back-EMF amplitude and calculate the rotor position.

The transfer function of DSOGI can be expressed as

$$H(s) = \frac{\hat{e}_{\alpha f}(s)}{\hat{e}_\alpha(s)} = \frac{k\omega s}{s^2 + k\omega s + \omega^2} \quad (14)$$

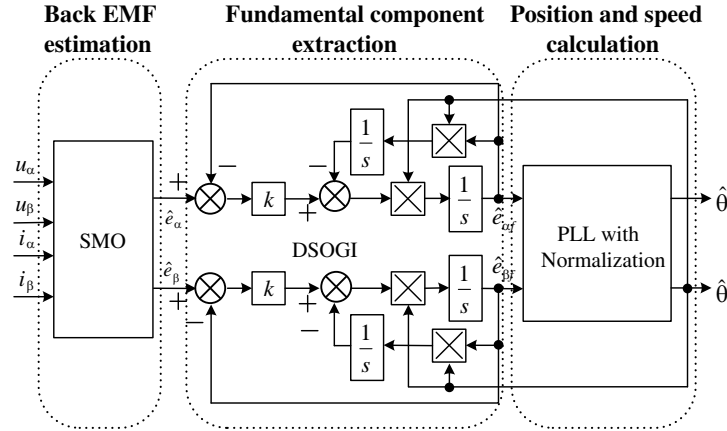


**Figure 5.** Block diagram of improved observer.

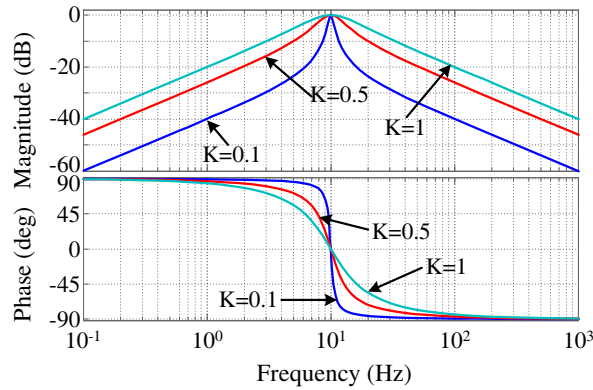


**Figure 6.** Frequency response of the SOGI.

where  $k$  is the adaption gain. Taking motor operating frequency  $\omega = 10$  Hz as an example, the frequency responses of the DSOGI are shown as Figure 6. It can be seen that the proposed strategy can extract the fundamental component effectively. Consequently, the harmonics contained in estimated back-EMF can be eliminated and the accuracy of estimated rotor position can be enhanced.

#### 4. EXPERIMENTAL VALIDATION

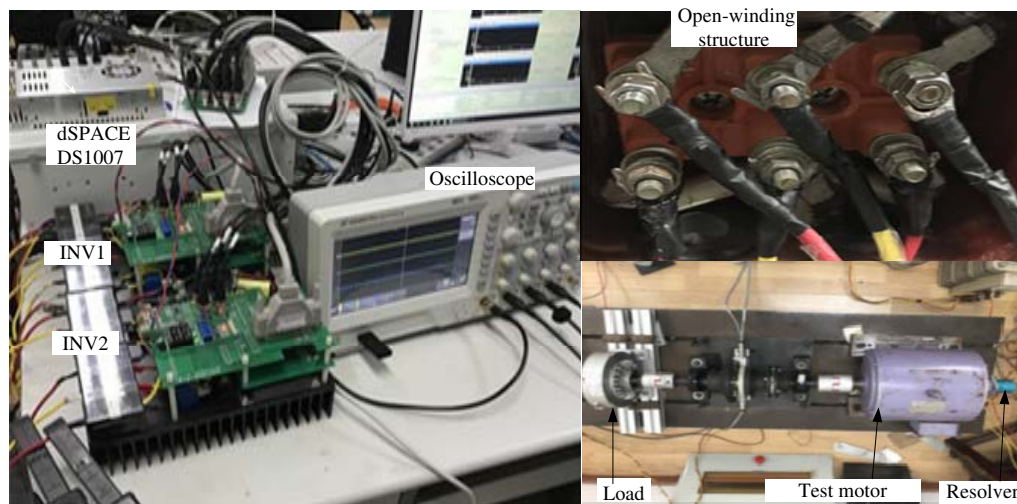
Figure 7 shows the platform of open-winding permanent magnet brushless motor, which is used to verify the effectiveness of the proposed strategy. Table 1 shows the main parameters of the motor. DS1007 dSPACE is utilized as the controller. The resolver is used to detect the actual rotor position for comparing with the estimated position. To evaluate the performance of the improved system, the experimental results of the steady state and dynamic state are given, respectively.

Figure 8 shows the estimated back-EMF at 90 r/min. It can be seen from Figure 8(a) that the back-EMF estimation without DSOGI is non-sinusoidal, namely, the estimated back-EMF contains harmonics. From Figure 8(b), it is obvious that the back-EMF estimation with DSOGI is more sinusoidal than the original estimation without DSOGI. Therefore, the estimated back-EMF harmonics are reduced by the DSOGI.

The steady-state performance of the proposed strategy is presented in Figure 9 and Figure 10. Figure 9(a) shows the estimated rotor position and position error without DSOGI. Figure 9(b) shows the estimated rotor position and position error with DSOGI. It can be seen that the fluctuation error is reduced and the position estimation becomes smooth by using the DSOGI. The position error is reduced from 0.2 rad to 0.07 rad. As the speed decreases, the operation of the motor becomes more and more

**Table 1.** The parameters of test motor.

Parameter/Unit	Value
rated power/kW	2.5
rated speed/(r/min)	1200
pole pairs	5
Ld/mH	3.707
Lq/mH	5.308
PM flux/Wb	0.129
phase resistance/ $\Omega$	0.239



**Figure 7.** Experimental platform.

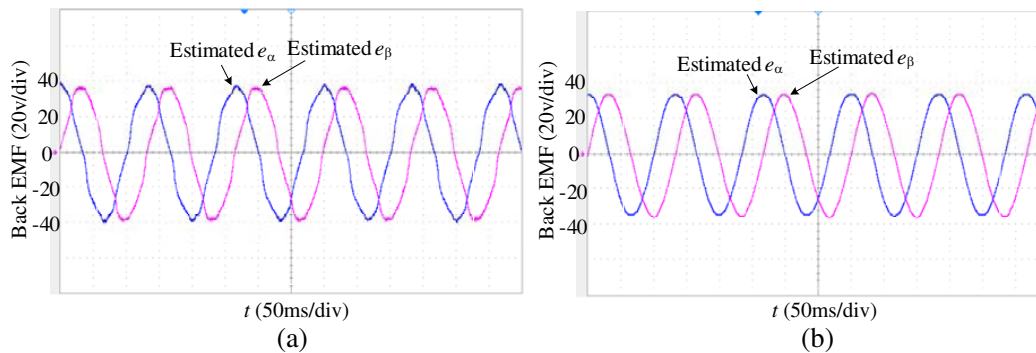


**Figure 8.** Back-EMF estimation without and with the DSOGI at 90 r/min. (a) Without DSOGI. (b) With DSOGI.

unstable. For sensorless control at low speeds, the high frequency injection method can be used. With speed increasing, the observer performance will be better. The fluctuation of the estimation error can be decreased. As can be seen from Figure 10, when the speed increases to 360 r/min, the error is very small.

The dynamic performance of the proposed strategy is shown in Figure 11 and Figure 12. The position error during speed changed from 100 r/min to 500 r/min is presented in Figure 11. It can be

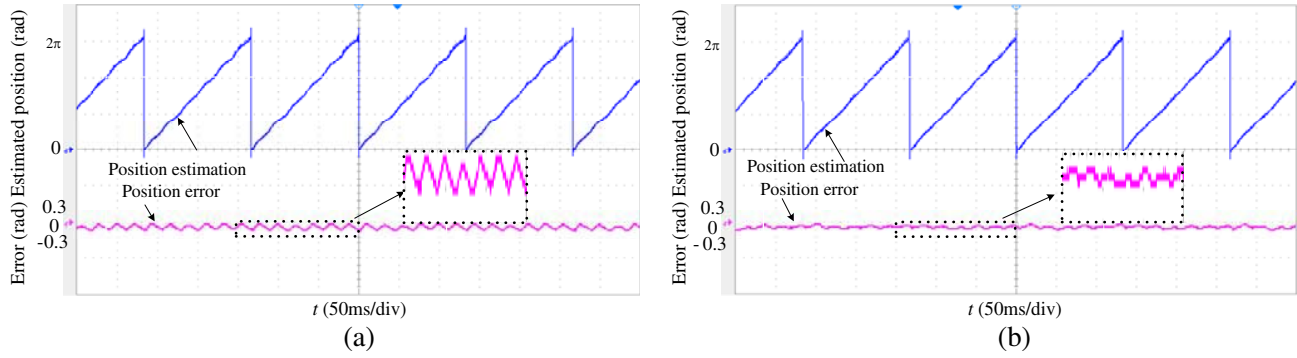


**Figure 9.** Position estimation and position error at 90 r/min. (a) Without DSOGI. (b) With DSOGI.

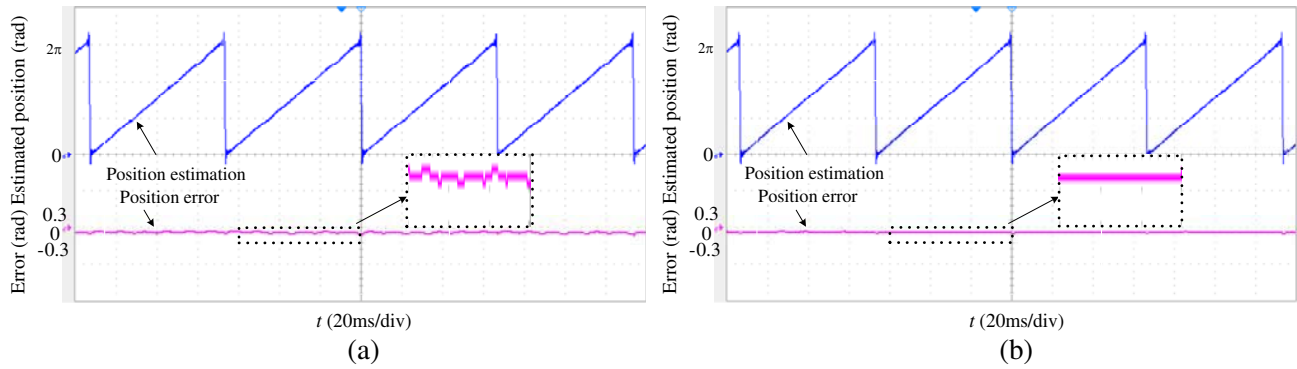


**Figure 10.** Position estimation and position error at 360 r/min. (a) Without DSOGI. (b) With DSOGI.

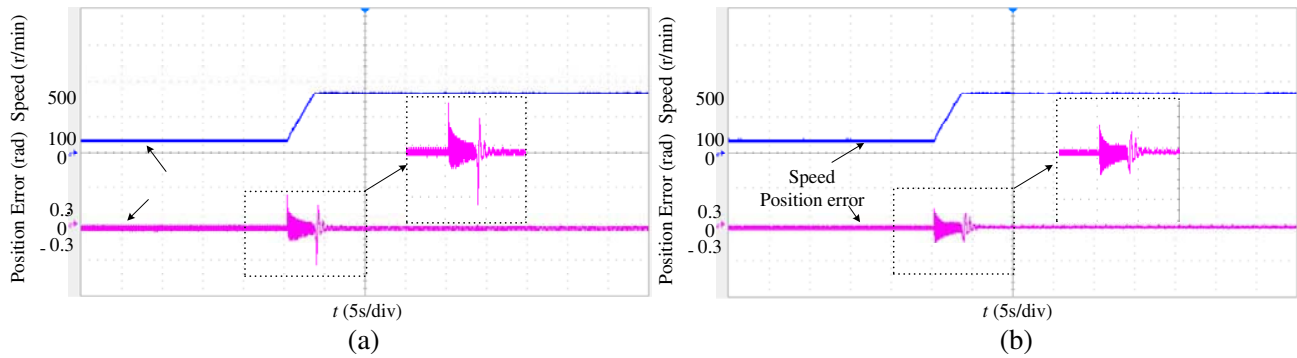


**Figure 11.** Speed tracking ability from 100 r/min to 500 r/min. (a) Without DSOGI. (b) With DSOGI.

seen that the position error has been reduced from about 0.6 rad to 0.3 rad by the proposed DSOGI. The system shows better speed tracking performance.

Furthermore, the disturbance rejection ability of drive system is shown in Figure 12. Figures 12(a) and (b) present the speed error, position error and phase current comparison without and with DSOGI, respectively. The load disturbance is changed from 20% to 100% rate load. The comparing results show that the disturbance rejection performance of drive system with DSOGI is obviously improved.

Therefore, the experimental results verify that the proposed strategy for the sensorless controlled open-winding permanent magnet brushless motor has better performance of steady-state and dynamic state.

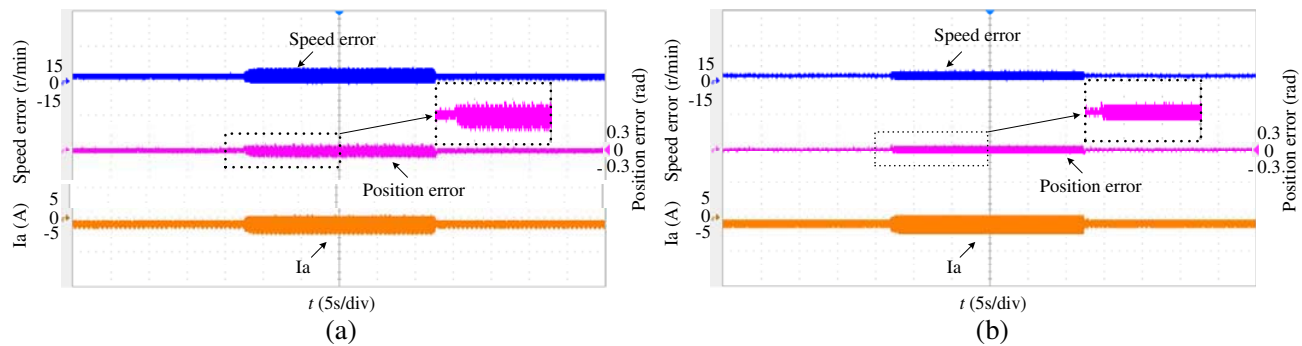


**Figure 12.** Disturbance rejection ability at 150 r/min. (a) Without DSOGI. (b) With DSOGI.

## 5. CONCLUSION

In this paper, a revised rotor position observer based on SMO with DSOGI is proposed for a sensorless controlled open-winding permanent magnet brushless motor, whose estimated back-EMF exhibits non-sinusoidal characteristics, in the medium and high speed range (from 90 r/min to rated speed). The DSOGI is utilized to extract the fundamental wave of back-EMF. The software quadrature PLL with back-EMF normalization is adopted to calculate the rotor position. Therefore, the accuracy of estimated rotor position can be enhanced. The effectiveness of the proposed method is validated by the comparison of experimental results. Although the improved sensorless control strategy is applied to the open-winding permanent magnet brushless motor, it is also applicable to other permanent magnet motors which need to suppress the estimated back-EMF harmonics.

## ACKNOWLEDGMENT

This work was supported in part by the National Natural Science Foundation of China under grant Nos. 51377073 and 51477069, in part by the Research Innovation Program for College Graduates of Jiangsu Province under grant No. KYLX16\_0895, and in part by the Priority Academic Program Development of Jiangsu Higher Education Institutions.

## REFERENCES

1. Liu, C. and K.-T. Chau, "Electromagnetic design and analysis of double-rotor flux-modulated permanent-magnet machines," *Progress In Electromagnetics Research*, Vol. 131, 81–97, 2012.
2. Refaie, A. E., "Motors/generators for traction/propulsion applications: A review," *IEEE Veh. Technol. Mag.*, Vol. 8, No. 1, 90–99, 2013.
3. Zhu, X., Z. Xiang, L. Quan, W. Wu, and Y. Du, "Multi-Mode optimization design methodology for a flux-controllable stator permanent magnet memory motor considering driving cycles," *IEEE Trans. Ind. Electron.*, Vol. 65, No. 7, 5353–5366, Jul. 2018.
4. Zhao, W., M. Cheng, R. Cao, and J. Ji, "Experimental comparison of remedial single-channel operations for redundant flux-switching permanent-magnet motor drive," *Progress In Electromagnetics Research*, Vol. 123, 189–204, 2012.
5. Nian, H. and Y. Zhou, "Investigation of open-winding pmsg system with the integration of fully controlled and uncontrolled converter," *IEEE Transactions on Industry Applications*, Vol. 51, No. 1, 429–439, 2015.
6. Kiadehi, A. D., K. E. K. Drissi, and C. Pasquier, "Angular modulation of dual-inverter fed open-end motor for electrical vehicle applications," *IEEE Transactions on Power Electronics*, Vol. 31, No. 4, 2980–2990, 2016.

7. Yang, S. C. and Y. L. Hsu, "Full speed region sensorless drive of permanent-magnet machine combining saliency-based and back-EMF-based drive," *IEEE Transactions on Industrial Electronics*, Vol. 64, No. 2, 1092–1101, 2017.
8. Gu, C., X. Wang, X. Shi, et al., "A PLL-based novel commutation correction strategy for a high-speed brushless DC motor sensorless drive system," *IEEE Transactions on Industrial Electronics*, Vol. 65, No. 5, 3752–3762, 2018.
9. Sun, Y., M. Preindl, S. Sirouspour, et al., "Unified wide-speed sensorless scheme using nonlinear optimization for IPMSM drives," *IEEE Transactions on Power Electronics*, Vol. 32, No. 8, 6308–6322, 2017.
10. Robert, W. H. and R. D. Lorenz, "Evaluating the practical low speed limits for back-EMF tracking-based sensorless speed control using drive stiffness as a key metric," *IEEE Transactions on Industry Applications*, Vol. 47, No. 3, 1337–1343, 2011.
11. Dai, N., R. Dutta, M. F. Rahman, et al., "Performance of a sensorless controlled concentrated-wound interior permanent-magnet synchronous machine at low and zero speed," *IEEE Transactions on Industrial Electronics*, Vol. 63, No. 4, 2016–2026, 2016.
12. Saadaoui, O., A. Khlaief, M. Abassi, et al., "A sliding-mode observer for high-performance sensorless control of PMSM with initial rotor position detection," *International Journal of Control*, Vol. 90, No. 2, 377–392, 2017.
13. Aydogmus, O. and M. F. Talu, "Comparison of extended-kalman- and particle-filter-based sensorless speed control," *IEEE Transactions on Instrumentation & Measurement*, Vol. 61, No. 2, 402–410, 2012.
14. Tang, Z. and B. Akin, "Suppression of dead-time distortion through revised repetitive controller in PMSM drives," *IEEE Transactions on Energy Conversion*, Vol. 32, No. 3, 918–930, 2017.
15. Lin, T. C., Z. Q. Zhu, and J. M. Liu, "Improved rotor position estimation in sensorless-controlled permanent-magnet synchronous machines having asymmetric-EMF with harmonic compensation," *IEEE Transactions on Industrial Electronics*, Vol. 62, No. 10, 6131–6139, 2015.
16. Zhang, G., G. Wang, D. Xu, et al., "Multiple-AVF cross-feedback-network-based position error harmonic fluctuation elimination for sensorless IPMSM drives," *IEEE Transactions on Industrial Electronics*, Vol. 63, No. 2, 821–831, 2016.
17. Yan, Z., H. He, J. Li, et al., "Double fundamental frequency PLL with second order generalized integrator under unbalanced grid voltages," *Journal of Power Supply*, 108–113, 2014.
18. Xavier, L. S., A. F. Cupertino, J. T. D. Resende, et al., "Adaptive current control strategy for harmonic compensation in single-phase solar inverters," *Electric Power Systems Research*, Vol. 142, 84–95, 2017.
19. Chen, C. Z., T. Mutuwo, D. Shinji, et al., "An extended electromotive force model for sensorless control of interior permanent-magnet synchronous motors," *IEEE Transactions on Industrial Electronics*, Vol. 50, No. 2, 288–295, 2003.